# Production of Degenerate Fermi Gases of $^6$Li Atoms in an Optical Dipole Trap

Xiang-Chuan Yan(严祥传)[1,3], Da-Li Sun(孙大立)[1*], Lu Wang(王璐)[1,3], Jing Min(闵靖)[1,3], Shi-Guo Peng(彭世国)[1], and Kai-Jun Jiang(江开军)[1,2*]

[1]*State Key Laboratory of Magnetic Resonance and Atomic and Molecular Physics, Wuhan Institute of Physics and Mathematics, Innovation Academy for Precision Measurement Science and Technology, Chinese Academy of Sciences, Wuhan 430071, China*

[2]*Center for Cold Atom Physics, Chinese Academy of Sciences, Wuhan 430071, China*

[3]*University of Chinese Academy of Sciences, Beijing 100049, China*

(Received 6 February 2021; accepted 9 March 2021; published online 2 May 2021)

We report the experimental production of degenerate Fermi gases of $^6$Li atoms in an optical dipole trap. The gray-molasses technique is carried out to decrease the atomic temperature to 57 μK, which facilitates the efficient loading of cold atoms into the optical dipole trap. The Fermi degeneracy is achieved by evaporative cooling of a two-spin mixture of $^6$Li atoms on the Feshbach resonance. The degenerate atom number per spin is $3.5 \times 10^4$, and the reduced temperature $T/T_{\rm F}$ is as low as 0.1, where $T_{\rm F}$ is the Fermi temperature of the non-interacting Fermi gas. We also observe the anisotropic expansion of the atom cloud in the strongly interacting regime.

DOI: 10.1088/0256-307X/38/5/056701

Ultracold atomic Fermi gases have unique advantages, such as tunable interaction, cleanness, and rich degrees of freedom. A degenerate Fermi gas of atoms can be studied in various ways with the development of experimental technologies. For example, using the Feshbach resonance to tune the inter-atomic interaction,[1] one can explore many-body physics in the crossover of Bose–Einstein condensation (BEC) of diatomic molecules and Bardeen–Cooper–Schrieffer (BCS) superfluid of fermionic pairs.[2,3] In the unitary region where the s-wave scattering length between atoms approaches to infinity and the behavior of the Fermi system will not depend on the details of the atomic potential, one can study the universality of atoms.[4−6] The optical dipole trap (ODT) and optical lattice are also powerful methods for studying the strongly correlated effects in ultracold Fermi gases.[7,8] In addition, a spin-imbalanced Fermi gas can be realized by adjusting the relative population of spin components in the system,[9,10] which has been a hot research topic in ultra-cold atomic physics.[11−18]

The degeneracy of Fermi gases was first realized in 1999.[19] Since then, research in this field has shown growing vitality. Especially in recent years, a series of novel macroscopic quantum phenomena have been discovered, including superfluid phase transition,[20] scale-invariant expansion,[21] formation of matter-wave soliton,[22] and so on. These phenomena exist in different systems, involving basic physics problems in the intersection of condensed matter physics, particle physics, and atomic and molecular physics. Meanwhile, to get a quantum system with fermions for studying many-body physics, the first task is to achieve a degeneracy of Fermi gases.

In this work, we experimentally achieve the quantum degeneracy of $^6$Li atoms in a crossed ODT. To efficiently load cold atoms into the ODT, the gray molasses process is carried out to decrease the temperature and increase the phase space density (PSD) (see Table 1), which is valid on Li atoms for sub-Doppler cooling. We then perform the evaporative cooling of a two-spin mixture of $^6$Li atoms on the Feshbach resonance in the ODT. Finally, we produce ultracold atoms at $T/T_{\rm F} = 0.1$, where $T_{\rm F}$ is the Fermi temperature of the non-interacting Fermi gas. The degenerate atom number per spin is about $3.5 \times 10^4$. We also observe the anisotropic expansion of the atom cloud in the strongly interacting regime. Following this work, we will study the non-equilibrium dynamic behaviors of strongly interacting Fermi gases.

The experimental setup is shown in Fig. 1. The vacuum chamber is composed of three parts: the effusive atomic oven, Zeeman slower and science chamber, as shown in Fig. 1(a). The vacuum pressure in the effusive oven is in the order of $10^{-8}$ Pa at room temperature, and will increase to the order of $10^{-6}$ Pa with a temperature of 450 ℃ during the experimental progress. A differential tube (an inner diameter of 5 mm and a length of 50 mm) between the effusive oven and Zeeman slower keeps the pressure of the science

Supported by the National Key Research and Development Program of China (Grant No. 2016YFA0301503), the National Natural Science Foundation of China (Grant Nos. 11674358, 11434015, and 11974384), the Chinese Academy of Sciences (Grant No. YJKYYQ20170025), and K. C. Wong Education Foundation (Grant No. GJTD-2019-15).

*Corresponding authors. Email: dlsun@wipm.ac.cn; kjjiang@wipm.ac.cn

chamber to the order of $10^{-9}$ Pa. An electromagnetic shutter is used for blocking the atomic beam after the Zeeman slowing process.

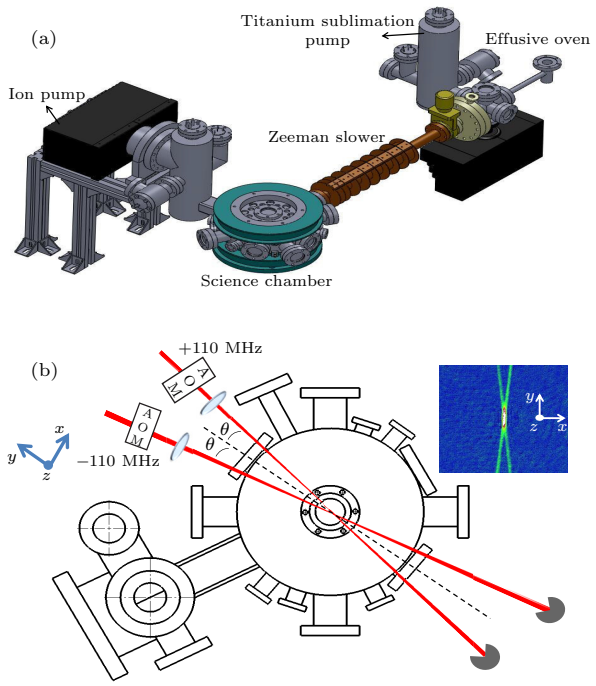


**Fig. 1.** Schematics of the experimental setup. (a) The vacuum chamber is composed of three parts, including the effusive atomic oven, Zeeman slower and science chamber. The ion pump and Titanium sublimation pump are used to produce and maintain the high vacuum pressure. (b) Configuration of the ODT. Two high-power laser beams intersect in the center of the science chamber at an angle of $2\theta = 11.3°$. Two AOMs work at +110 MHz and −110 MHz, respectively, to avoid optical interference. The inset is an example of an image of an atomic cloud in the ODT.

We employ the magneto-optical trap (MOT), compressed magneto-optical trap (C-MOT) and gray molasses as the three sequential steps of the laser cooling. The atomic temperature, number, and cloud size can be measured from the time of flight (TOF) images, and then the atomic density and phase space density (PSD) can be calculated. The experimental parameters and relevant results during the laser cooling are summarized in Table 1.

The atomic beam emitted from the effusive oven is Zeeman slowed and then collected in the MOT. We use one diode laser as the seeding laser and four tapered amplifiers (TAs) to provide enough laser power for Zeeman slowing and laser cooling. The frequency of the diode laser is stabilized using the standard saturation absorption spectrum (SAS). The Zeeman slowing beam has a power of 90 mW and a red detuning of 170 MHz from the D2 line transition $|2^2S_{1/2}, F = 3/2\rangle \rightarrow |2^2P_{3/2}, F'\rangle$. In the MOT, the cooling light (repumping light) has a red detuning of $-6.8\Gamma$ ($-5.1\Gamma$) from the D2 line transition $|2^2S_{1/2}, F = 3/2\rangle \rightarrow |2^2P_{3/2}, F'\rangle$ ($|2^2S_{1/2}, F = 1/2\rangle \rightarrow |2^2P_{3/2}, F'\rangle$), where $\Gamma = 5.8$ MHz is the natural linewidth of the excited state.[23] The cooling and repumping beams are combined into the same optical fiber, and then the output constructs three pairs of laser beams with the retro-reflection configuration. Each pair has a power of 20 mW for the cooling light and 5 mW for the repumping one. The waist radius of the cooling beam is 8 mm. After loading atoms into the MOT for about 20 s, we perform the C-MOT for about 3 ms to further decrease the atomic temperature. In this process, the power of the cooling light as well as the repumping one is linearly reduced to 10% of its initial value, respectively, and the frequency detuning is decreased to $-3\Gamma$ for both. The magnetic field gradient is linearly increased from 24 G/cm to 45 G/cm, compressing the atomic cloud. After the C-MOT, though the atom number is lost some, the temperature is reduced from 4 mK to 500$\mu$K.

The standard optical molasses cooling on D2 line transition is not efficient for Li atoms because the separation between hyperfine structure levels of the excited state is smaller than the natural linewidth. Another kind of sub-Doppler cooling technique, termed gray molasses,[24−26] is valid on Li atoms. In our experiment, the cooling light for gray molasses has a blue detuning of $5\Gamma$ from the D1 line transition $|2^2S_{1/2}, F = 3/2\rangle \rightarrow |2^2P_{1/2}, F = 3/2\rangle$, as well as the repumping light with a blue detuning of $5\Gamma$ from the transition $|2^2S_{1/2}, F = 1/2\rangle \rightarrow |2^2P_{1/2}, F = 3/2\rangle$. The gray molasses lasts for 2 ms after switching off the magnetic field of the C-MOT. The laser beams for the gray molasses overlap with those of the MOT, which facilitates the optical alignment. After the gray molasses, the atomic temperature is reduced to 57 μK with about one order of magnitude smaller, and the phase space density (PSD) is increased by a factor of 24 (see Table 1).

**Table 1.** Experimental parameters and relevant results during the laser cooling. Here $\delta_{\rm cooling}$ ($\delta_{\rm repumping}$) is the detuning of the cooling light (repumping light), $N$ is the atom number, $n$ is the atomic density in the center, $T$ is the atomic temperature, and PSD $= n\lambda^3$ is the phase space density with $\lambda$ being the de Broglie wavelength. $\Gamma$ is the natural linewidth of the excited state.

| Parameter | MOT | C-MOT | Gray molasses |
|---|---|---|---|
| $\partial B_z/\partial z$ | 24 G/cm | 45 G/cm | 0 G/cm |
| $\delta_{\rm cooling}$ | $-6.8\ \Gamma$ | $-3\ \Gamma$ | $5\ \Gamma$ |
| $\delta_{\rm repumping}$ | $-5.1\ \Gamma$ | $-3\ \Gamma$ | $5\ \Gamma$ |
| $N$ | $1.0\times10^9$ | $5\times10^8$ | $3\times10^8$ |
| $n$ (cm$^{-3}$) | $1.0\times10^{10}$ | $9.8\times10^{10}$ | $7.3\times10^{10}$ |
| $T$ | 4 mK | 500 μK | 57 μK |
| PSD | $1.42\times10^{-8}$ | $2.5\times10^{-6}$ | $6.2\times10^{-5}$ |

To achieve the degenerate Fermi gases, we load cold atoms into an ODT for evaporative cooling. The laser beam of the ODT is provided by a single-mode ytterbium-doped IPG fiber laser (YLR-200-1064-LP-WC). The ODT light is tuned on 200 ms ahead of

the end of the MOT. A 10 μs hyperfine pumping to the state $|F = 1/2\rangle$ is achieved by tuning off the repumping light of the gray molasses before the cooling light. The population ratio of the two spin states ($|F = 1/2, m_F = -1/2\rangle$ and $|F = 1/2, m_F = 1/2\rangle$) is in the range of $40:60 \sim 50:50$. The configuration of the ODT is shown in Fig. 1(b). Two laser beams are focused and intersect in the science chamber at an angle of 11.3°. The waist radius of the laser beam is 38 μm. Two acousto-optical modulators (AOMs) used to control the laser beams work at frequencies of +110 MHz and −110 MHz, respectively, for avoiding optical interference. The atomic cloud loaded into the ODT is shown in the inset of Fig. 1(b). The lifetime of cold atoms in the ODT is measured to be about 25 s at $B = 0$ G.

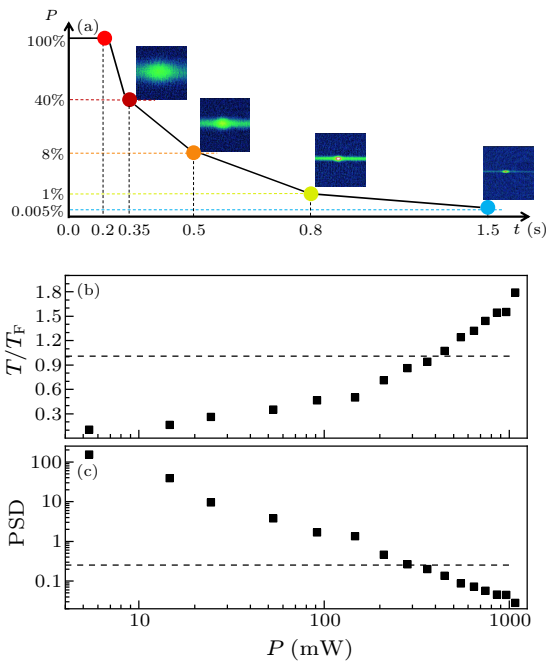


**Fig. 2.** Evaporative cooling in the ODT. (a) The time sequence of the evaporative cooling. The initial laser power $P$ is set to 100%. The process of ramping down the laser power is divided into four stages. The representative atomic cloud in the end of each stage is also shown, illuminating the decreasing of the atomic cloud size and increasing of the atomic density. (b) The reduced temperature $T/T_F$ versus the laser power $P$. The dashed line denotes the Fermi temperature $T_F$. (c) The phase space density (PSD) versus the laser power $P$. The dashed line denotes the PSD with a value of 1, indicating the quantum degeneracy of the Fermi gas. It is noted that the axes are logarithmically plotted.

We carry out the evaporative cooling at $B = 832$ G, where the s-wave scattering length is infinitely large. The lifetime of cold atoms is measured to be about 7 s, which is long enough for evaporative cooling. The time sequence of the evaporative cooling is shown in Fig 2(a). The ODT light is firstly turned on with a power of 70 W for each beam and kept for about 0.2 s for equilibrium. The initial atom number in the ODT is about $1.0 \times 10^6$. We then ramp down the laser power by four-stage linear scanning and with a period of about 1.5 s. The percentage of the laser power is monitored by a photo detector. For the first two stages, the laser power is controlled by an external voltage. For the last two stages, a PID locking circuit is introduced to stabilize the optical intensity. At the laser power $P = 144$ mW, we measure the trapping frequencies of the ODT using the parametric heating method, where $\omega_z \approx \omega_x \approx 2\pi \times 750.8$ Hz and $\omega_y \approx 2\pi \times 58.3$ Hz. The atomic temperature can be extracted by fitting the atomic density with a finite-temperature Fermi–Dirac distribution (see an example in Fig. 3).[27] We can then calculate the phase space density $\mathrm{PSD} = N(\hbar\bar{\omega}/k_B T)^3$, where $N$ is the atomic number, $\bar{\omega}$ is the geometric average trapping frequency and $T$ is the atomic temperature. With the laser power decreasing, the atomic temperature decreases and the PSD increases [see Figs. 2(b) and 2(c)]. The reduced temperature $T/T_F$ approaches 1 when the optical power is ramped down to about 400 mW. When the laser power is further ramped down to about 150 mW, the Fermi gases show a quantum degeneracy with PSD ≈1 and $T/T_F \approx 0.5$.

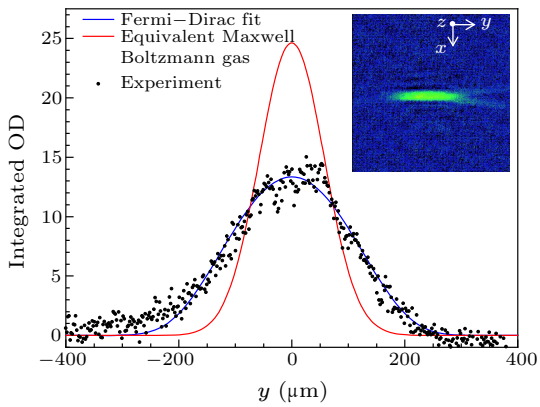


**Fig. 3.** Integrated optical density (OD) in $y$-direction (along the axial direction). The atomic cloud is *in situ* imaged at 832 G. The laser power of the ODT is 5.4 mW. The experimental data are fitted by a finite-temperature Fermi–Dirac distribution (blue curve). A small reduced temperature $T/T_F = 0.1$ is extracted. As a comparison, an equivalent Maxwell–Boltzmann classical gas (red curve) is plotted with the same atomic temperature and number. The inset denotes the image of the atomic cloud.

When the Fermi gases reach quantum degeneracy, the Maxwell–Boltzmann gas is no longer applicable to describe the system, and the atomic density satisfies the Fermi–Dirac distribution. The atomic cloud is *in situ* imaged at 832 G and the integrated optical density in $y$-direction (along the axial direction) is shown in Fig. 3. The laser power of the ODT is only 5.4 mW, which corresponds to a trapping potential of 200 nK. We numerically fit the atomic density using a finite-temperature Fermi–Dirac distribution (polylogarithmic function),[27,28] extracting the reduced tem-

perature $T/T_{\rm F} = 0.1$. The degenerate atom number per spin is $3.5 \times 10^4$. For comparison, we also plot an equivalent Maxwell–Boltzmann classical gas (Gaussian distribution) with the same atomic temperature and number.[28,29] The quantum statistics results in a significant discrepancy from the classical gas. The atomic density distribution of the degenerate Fermi gas has a wider flat top than that of a classical gas, which is caused by the Pauli exclusion principle in the quantum regime.[30]

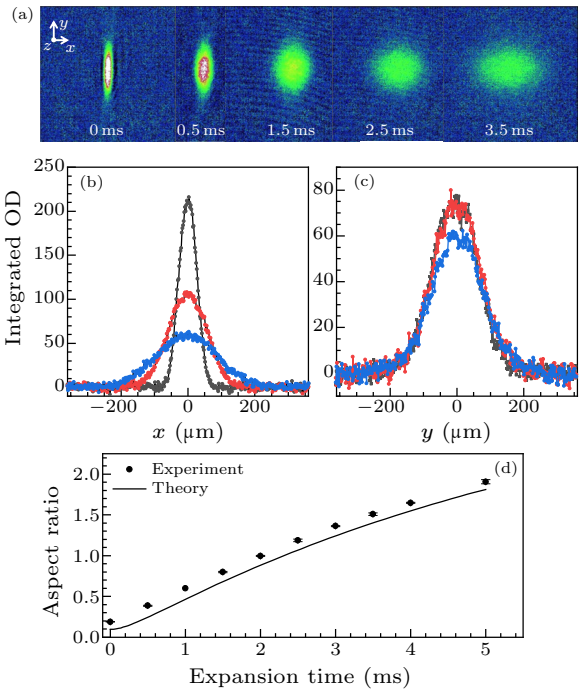


**Fig. 4.** Anisotropic expansion of the degenerate Fermi gases in the strongly interacting regime. (a) Exemplary atomic clouds during the expansion. $B = 832\,$G, $T/T_{\rm F} = 0.5$. The expansion time is from 0 ms to 3.5 ms. Integrated optical density in $x$-direction (along the radial direction) (b) and in $y$-direction (along the axial direction) (c). The expansion time is 0.5 ms (black), 1.5 ms (red) and 2.5 ms (blue), respectively. (d) The aspect ratio $(\sigma_x/\sigma_y)$ as a function of the expansion time. The error bar is smaller than the mark size. The solid curve is the theoretical calculation in the unitary regime.[31,32]

The expansion dynamics of strongly interacting Fermi gases has been used to measure the thermodynamic parameters of the system.[27] The degenerate Fermi gases released from an anisotropic trap will show a characteristic anisotropic expansion due to the many-body interaction.[33,34] We prepare a degenerate Fermi gas at $T/T_{\rm F} = 0.5$ and with an atom number of $1.3 \times 10^5$. To study the expansion behavior of the strongly interacting Fermi gases, we turn off the ODT and maintain the magnetic field at $B = 832\,$G. As shown in Fig. 4(a), the atomic cloud is probed for different expansion times, where the anisotropic expansion is obvious. The atomic cloud expands rapidly along the radial direction [Fig. 4(b)], while it remains nearly unchanged along the axial direction [Fig. 4(c)]. The atomic cloud size $(\sigma_x, \sigma_y)$ can be measured by fitting the atomic density with a Fermi–Dirac distribution. The aspect ratio $(\sigma_x/\sigma_y)$ during the expansion is plotted in Fig. 4(d), and exceeds 1 with a short expansion time of 2.0 ms. The theoretical calculation for the hydrodynamic expansion in the unitary regime[31,32] agrees well with the experimental results. This behavior is in contrast to the non-interacting expansion, for which the aspect ratio never exceeds 1.

In conclusion, we experimentally produce the degenerate two-spin Fermi gases of $^6$Li atoms in an ODT. The gray molasses technique is demonstrated to be valid on Li atoms for sub-Doppler cooling, which facilitates the efficient loading of cold atoms into the ODT. A deep degeneracy at $T/T_{\rm F} = 0.1$ is achieved by evaporative cooling of a two-spin mixture on the Feshbach resonance. The anisotropic expansion has been observed for the Fermi gases in the unitary region. This work builds a good starting point to explore the many-body physics in the BEC-BCS crossover and non-equilibrium dynamics of strongly interacting Fermi gases.

## References

[1] Chin C, Grimm R, Julienne P and Tiesinga E 2010 *Rev. Mod. Phys.* **82** 1225
[2] Bourdel T, Khaykovich L, Cubizolles J, Zhang J and Chevy F 2004 *Phys. Rev. Lett.* **93** 050401
[3] Chin C, Bartenstein M, Altmeyer A, Riedl S and Jochim S 2004 *Science* **305** 1128
[4] Pollack S E, Dries D and Hulet R G 2009 *Science* **326** 1683
[5] Nascimbene S, Navon N, Jiang K J, Chevy F and Salomon C 2010 *Nature* **463** 1057
[6] Peng S G, Zhang C X, Tan S and Jiang K 2018 *Phys. Rev. Lett.* **120** 060408
[7] Giorgini S, Pitaevskii L P and Stringari S 2008 *Rev. Mod. Phys.* **80** 1215
[8] Li J, Harter A K, Liu J, de Melo L and Joglekar Y N 2019 *Nat. Commun.* **10** 855
[9] Gupta S, Hadzibabic Z, Zwierlein M, Stan C and Dieckmann K 2003 *Science* **300** 1723
[10] Qi W, Liang M C, Zhang H, Wei Y D and Wang W W 2019 *Chin. Phys. Lett.* **36** 093701
[11] Zwierlein M W, Schirotzek A, Schunck C H and Ketterle W 2006 *Science* **311** 492
[12] Partridge G B, Li W, Kamar R I, Liao Y A and Hulet R G 2006 *Science* **311** 503
[13] Iskin M and Subaşı A 2011 *Phys. Rev. Lett.* **107** 050402
[14] Mendoza R, Fortes M, Solís M and Koinov Z 2013 *Phys. Rev. A* **88** 033606
[15] Revelle M C, Fry J A, Olsen B A and Hulet R G 2016 *Phys. Rev. Lett.* **117** 235301
[16] Nascimbène S, Navon N, Jiang K J, Tarruell L and Teichmann M 2009 *Phys. Rev. Lett.* **103** 170402
[17] Peng S G, Tan S and Jiang K 2014 *Phys. Rev. Lett.* **112** 250401
[18] Chen Q, Wang J, Sun L and Yu Y 2020 *Chin. Phys. Lett.* **37** 053702
[19] DeMarco B and Jin D S 1999 *Science* **285** 1703
[20] Zwierlein M W, Schunck C H, Schirotzek A and Ketterle W 2006 *Nature* **442** 54
[21] Deng S, Shi Z Y, Diao P, Yu Q and Zhai H 2016 *Science* **353** 371

[22] Strecker K E, Partridge G B, Truscott A G and Hulet R G 2002 *Nature* **417** 150
[23] McAlexander W, Abraham E and Hulet R 1996 *Phys. Rev. A* **54** R5
[24] Fernandes D R, Sievers F, Kretzschmar N, Wu S and Salomon C 2012 *Europhys. Lett.* **100** 63001
[25] Sievers F, Kretzschmar N, Fernandes D R, Suchet D and Rabinovic M 2015 *Phys. Rev. A* **91** 023426
[26] Burchianti A, Valtolina G, Seman J A, Pace E and De Pas M 2014 *Phys. Rev. A* **90** 043408
[27] Kinast J, Turlapov A, Thomas J E, Chen Q and Stajic J 2005 *Science* **307** 1296
[28] Veeravalli G 2009 *PhD Thesis* (Swinburne University of Technology)
[29] Xiong D Z, Chen H X, Wang P J, Yu X D and Gao F 2008 *Chin. Phys. Lett.* **25** 843
[30] Truscott A G, Strecker K E, McAlexander W I, Partridge G B and Hulet R G 2001 *Science* **291** 2570
[31] Cao C, Elliott E, Joseph J, Wu H and Petricka J 2011 *Science* **331** 58
[32] Deng S J, Diao P P, Yu Q L and Wu H B 2015 *Chin. Phys. Lett.* **32** 053401
[33] O'hara K, Hemmer S, Gehm M, Granade S and Thomas J 2002 *Science* **298** 2179
[34] Kinast J, Hemmer S, Gehm M, Turlapov A and Thomas J 2004 *Phys. Rev. Lett.* **92** 150402